Equatorial broad plasma depletions associated with the enhanced fountain effect

Woo Kyoung Lee[1,2], Hyosub Kil[1], Young-Sil Kwak[2], Larry J. Paxton[1], Yongliang Zhang,[1], Ivan Galkin[3] and Inez S. Batista[4]

[1]The Johns Hopkins University Applied Physics Laboratory, Maryland, USA

[2]Korea Astronomy and Space Science Institute, Daejeon, South Korea

[3]University of Massachusetts Lowell, Massachusetts, USA

[4]National Institute of Space Research, São Paulo, Brazil

Abstract

Broad plasma depletions (BPDs), plasma depletions whose longitudinal width is over several hundred kilometers, have been detected in the equatorial *F* region by low-earth-orbit satellites during both magnetically quiet and magnetically disturbed periods. A few hypotheses were suggested to explain the creation of BPDs, but the underlying mechanism of this phenomenon is still under debate. We investigate the origin of BPDs by analyzing the simultaneous in situ and optical observations of the ionosphere on 30 May 2003 ($Kp = 8^{+}$), 24 April 2012 ($Kp = 7^{-}$), and 31 October 2012 ($Kp = 0^{+}$). A BPD on 30 May 2003 was detected by the Republic of China Satellite-1 at an altitude of 600 km, and BPDs on the other days were detected by the Communication/Navigation Outage Forecasting System satellite near an altitude of 400 km. Our results show that the detection of BPDs is closely associated with background ionospheric morphology; BPDs are detected on the days when the equatorial ionization anomaly (EIA) is intense and the crests of the EIA have moved poleward. Measurements of upward plasma motion further support the existence of ionospheric uplift at BPD locations. **On 29–30 May 2003, the uplift of the *F* peak height above an altitude of 700 km in the region where BPDs were detected is evidenced by an ionosonde observation.** These observations and the detection of BPDs near the magnetic equator lead to the interpretation that the satellite detection of BPDs during those three days is likely related to the uplift of the *F* peak height above the satellite orbits. Coincident observations of small-scale plasma depletions near the BPDs can be explained by enhanced likelihood of plasma instability caused by the ionospheric uplift.

1. Introduction

Plasma bubbles indicate plasma depletions relative to the background plasma density in the equatorial *F* region. Bubbles are a nighttime phenomenon and occur during both magnetically quiet and magnetically disturbed periods. The longitudinal width of bubbles is typically ~100 km [*Hei et al.*, 2005]. The latitudinal and altitudinal extents of bubbles vary depending on the bubbles' growth. Because plasma instability occurs in a whole magnetic flux tube, bubbles appear as elongated structures along the magnetic field lines. Steep plasma density gradients form on the bottomside of the *F* region after sunset, which leads to the growth of the Rayleigh-Taylor (R-T) instability [*Kelley*, 2009; *Sultan*, 1996]. Although bubbles are the dominant irregularity feature in the equatorial *F* region, sometimes abnormally large plasma depletions whose longitudinal width is over several hundred kilometers appear. We call those depletions broad plasma depletions (BPDs) to distinguish them from regular bubbles. BPDs may be considered a different type of bubble, but no study showed the creation of such broad bubbles by the R-T instability.

BPDs have been detected by various satellites during large geomagnetic storms [*Basu et al.*, 2001; *Burke et al.*, 2000, 2009; *Greenspan et al.*, 1991; *Kil and Paxton*, 2006; *Kil et al.*, 2006; *Lee et al.*, 2002; *Su et al.*, 2002]. For this reason, BPDs were considered to be a storm-time phenomenon. A rigorous investigation of the BPD phenomenon began from the report of BPDs detected by the Defense Meteorological Satellite Program F9 [*Greenspan et al.*, 1991]. The observation of large upward plasma drifts in the region where the BPD was detected led the authors to the conclusion that an extreme equatorial fountain process, caused by either the penetration electric fields or the disturbance dynamo electric fields, is responsible for the BPD. From the investigation of BPDs detected by the Republic of

China Satellite-1 (ROCSAT-1) at an altitude of 600 km, *Su et al*. [2002] reached a similar conclusion. However, *Kil and Paxton* [2006] noticed the coincidence of BPDs with bubbles and suggested that the consolidation of small-scale bubbles might form BPDs. *Burke et al*. [2000] understood the formation of BPDs in terms of the bubbles whose growth was accelerated by storm-induced electric fields.

Recent observations of Communication/Navigation Outage Forecasting System (C/NOFS) satellite show that BPDs occur during magnetically quiet as wells as magnetically disturbed periods. *Huang et al*. [2011] proposed that bubbles grow as time progresses and form BPDs by a merging process. This idea is similar to the explanation of storm-time BPDs by *Kil and Paxton* [2006]. To explain the creation of BPDs by a merger, bubbles are supposed to exist prior to the detection of BPDs. However, we noticed many BPDs that developed in regions where bubbles were absent prior to the detection of BPDs. **Using the coincident C/NOFS and radar observations over Jicamarca in Peru, *Kil and Lee* [2013] reported a BPD event that did not show an association with bubbles.** The C/NOFS satellite detected BPDs mostly near the magnetic equator and at low altitudes. In many cases, regular-size bubbles appear in the longitude regions where BPDs are detected when the satellite orbit moves slightly to higher latitudes or altitudes. These observations pose a question: Why is the merging process effective only near the magnetic equator and at low altitudes?

Frequent detection of BPDs near the magnetic equator when the C/NOFS is near perigee provides a clue to the origin of BPDs. Satellites have a greater chance of passing through the bottomside of the *F* region when their heights are low and when they cross the magnetic equator. As suggested by *Su et al*. [2002], detection of BPDs under those conditions can be understood in terms of the relationship between the satellite orbit and *F* region height. We extend the study of *Su et al*. [2002] by providing further supporting evidence for this view. To investigate the background ionospheric conditions when BPDs are detected, we have chosen BPD events on the days when simultaneous optical observations of the ionosphere were available. These conditions occurred on 30 May 2003 and 24 April 2012 (magnetically disturbed periods) as well as on 31 October 2012 (magnetically quiet period). A BPD on 30 May 2003 was detected by ROCSAT-1, and BPDs on the other days were detected by the Coupled Ion-Neutral dynamics Investigation (CINDI) instrument onboard the C/NOFS satellite. The measurements of the atomic oxygen (OI) 135.6 nm intensity from the Global Ultraviolet Imager (GUVI) onboard Thermosphere–Ionosphere–Mesosphere Energetics and Dynamics (TIMED) satellite are available on 30 May 2003, and the observations from the Special Sensor Ultraviolet Spectrographic Imager (SSUSI) onboard Defense Meteorological Satellite Program (DMSP) F18 are available on the other two days. GUVI and SSUSI observations are used for the investigation of the severity of the fountain process (or uplift of the ionosphere) and for the identification of the existence of bubbles at the locations of BPDs. **The measurements of the ion density by the CHAllenging Minisatellite Payload (CHAMP) satellite and the ionosonde observations at São Luis (2.5°S, 44.3°W) in Brazil are also used to support the GUVI observations on 30 May 2003.**

2. Data

ROCSAT-1 was launched in March 1999 at an altitude of 600 km, and its orbital inclination was 35°. The ROCSAT-1 mission was ended in June 2004. The C/NOFS satellite, launched in 2008, has an orbit inclination of 13°, and its orbit altitude varies from 400 km (perigee) to 850 km (apogee). The CHAMP satellite was initially launched into near polar orbit with an altitude of 454 km and an inclination of 87°. Its mission was over in September 2010. The altitude of CHAMP in 2003 was near 400 km. This study uses the measurements of the ion density and vertical velocity by the Ionospheric Plasma and

Electrodynamics Instrument (IPEI) onboard ROCSAT-1 and C/NOFS/CINDI and the measurements of the ion density by the Planar Langmuir Probe (PLP) onboard CHAMP.

TIMED satellite has a circular orbit at an altitude of 630 km with an inclination of 74°. The GUVI instrument onboard the TIMED satellite observes spectral images of far ultraviolet (FUV) airglow with five colors (HI 121.6 nm, OI 130.4 nm, OI 135.6 nm, N_2 Lyman-Birge-Hopfield (LBH) from 140.0 to 150.0 nm (LBHS) and from 165.0 nm to 180 nm (LBHL)) [*Christensen et al*., 2003; *Paxton et al.*, 1999; 2004]. SSUSI is the previous generation spectrometer observing FUV airglow carried by sun-synchronous DMSP satellites at an altitude of 830 km [*Paxton et al.*, 1992a, 1992b, 2002]. The GUVI and SSUSI instruments use a cross-track scanning mirror to produce horizon-to-horizon and limb images of the ionosphere and thermosphere. This study uses the disk-scan images of OI 135.6 nm intensity at night.

3. Results and discussion

3.1 Observations on 29–30 May 2003

Intense geomagnetic disturbances were recorded on 29–30 May 2003. The Dst index reached -144 nT at 2300 UT on the 29th, and it stayed below -100 nT until 0400 UT on the 30th. The peak Kp value was 8^+ at 1800–2400 UT on the 29th. The CHAMP satellite detected plasma depletions about 30° wide in latitude on four consecutive orbits in the African, Atlantic, and American sectors during the storm period. Figure 1 presents the CHAMP observations at 0200 LT. The ground tracks of the CHAMP satellite and the UTs of the satellite pass at the geographic equator are shown in Figure 1a. The electron densities along the CHAMP obits are shown in Figure 1b. The colors of the density and orbits are arranged to match. Broad plasma depletions are detected in the equatorial region on the orbits between

1.8 and 6.4 UT. **Those depletions are indicated with thick lines in the orbit and density plots.** Although BPDs are defined on the basis of the longitudinal width of the depletions, latitudinally broad depletions may also be categorized as BPDs because those depletions are abnormally wide compared with typical bubbles. The densities at 0.3 UT (black dotted curve) are shown as a reference for the latitudinal density profile in the region where BPDs are not detected. Along the orbit at 0.3 UT, the density peak occurs near the magnetic equator, and the equatorial ionization anomaly (EIA) feature does not appear. On the following orbits, BPDs are detected in the equatorial region, and the densities in low-middle latitudes are much greater than those at 0.3 UT. The formation of deep plasma depletions at the magnetic equator simultaneously with the intensification of the EIA can be explained by the occurrence of a severe fountain process or uplift of the ionosphere. On the density plot at 1.8 UT (red curve in Figure 1b), the latitudinal density variation is quite smooth with no irregularities. Thus bubbles do not seem to be involved in the formation of the depletion. Excluding bubbles as the source, the enhanced fountain process is the most likely mechanism for the formation of deep plasma depletion near the magnetic equator. However, bubbles are still the candidate cause of the BPDs on other orbits because small-scale irregularities accompany the BPDs. The role of bubbles in the creation of BPDs is further discussed in the following sections.

The CHAMP observations in Figure 1 show the increase of the latitudinal width of BPDs as time progresses or as the satellite orbit moves westward; the BPD detected at 6.4 UT over South America is the widest (blue thick curve) and the BPD detected at 1.8 UT over Africa is the narrowest (red thick curve). If the formation of the BPDs detected by CHAMP is associated with the enhanced fountain process, the EIA morphology would show a similar longitudinal variation. The GUVI OI 135.6 nm intensity map provides a tool for testing the severity of the fountain process and its longitudinal variation.

Figure 2 presents GUVI OI 135.6 nm intensity maps on the nights of (a) the 28th through 29th (before the storm) and (b) the 29th through 30th (during the storm) May 2003. Time progresses from right to left, and UTs at the time of the satellite passes at the geographic equator are given on the top of each map. The GUVI observation LT is around 2200. The OI 135.6 nm intensity maps represent the square of the height-integrated electron density up to the satellite altitude. To provide a longitudinally continuous view of the ionospheric morphology, the intensity is projected onto an altitude of 150 km instead of onto a more realistic *F* peak altitude. The intensity map projected onto an altitude of 350 km is shown in Figure 3. The distinctive behavior of the ionosphere during the storm period is observed in the auroral and EIA regions. The intensification and equatorward expansion of the aurora (bright arcs in high latitudes) during the storm period is clearly visible. At low latitudes, the EIA intensity is strengthened and the northern and southern EIAs are farther separated during the storm period. These low latitude changes are most severe in the American sector. The EIA morphology observed by GUVI demonstrates the existence of an enhanced fountain process in the African–American sectors, especially in the American sector during the storm period. **The thick white lines in Figure 2b indicate the BPD locations shown in Figure 1.** The detection of wider BPDs closer to the American sector is consistent with the observation of farther separations of the northern and southern EIAs closer to the American sector. In Figure 2b, one may notice overall enhancements of the OI 135.6 nm intensity from the auroral region to the equatorial region between 2000 and 0340 UT. This time period corresponds to the period of main phase and large negative Dst index. This brightening of the nightglow is explained by the effect of the precipitation of energetic neutral atoms originating from the ring current [*Zhang et al.*, 2006].

During the 29–30 May 2003 storm, BPDs are detected even at an altitude of 600 km over South America. The measurements of the ion density and vertical velocity by ROCSAT-1 provide further insight into the ionospheric conditions during the storm. Figure 3a shows the GUVI OI 135.6 nm map and ROCSAT-1 passes. The OI 135.6 nm intensity map is the same as Figure 2b except for the projection onto an altitude of 350 km. The ion densities and vertical ion velocities along the ROCSAT-1 orbits are shown in Figures 3b and 3c, respectively. Bubbles are detected over South America on orbit 2. Those depletions are detected at the magnetic latitude of 20°S. Bubble signatures are also seen on the OI 135.6 nm intensity map at the northern anomaly region (near 20°N geographic latitudes on the second swath from the left). They are considered to be the conjugate images of the bubbles detected on the ROCSAT-1 orbit 2. As the satellite orbit moves closer to the magnetic equator, wider depletions appear. The locations of those BPDs (red shaded regions) on orbits 3 and 4 are marked with thick lines in Figure 3a. The detection of wider depletions may be understood as a consequence of the temporal evolution of bubbles (for example, a merging process), but this phenomenon can also be understood in terms of the relationship between the *F* region height and satellite altitude. The latter idea is supported by the ROCSAT-1 detection of BPDs in the longitude region (South America) where the strongest fountain process, and therefore, the strongest uplift of the equatorial ionosphere occurred.

The measurements of the vertical ion velocity (upward is positive) on orbit 1 show the upward drift of the ionosphere between the longitudes of 300° and 340°E. On orbit 2, the vertical velocity is near zero in that region, and the vertical drift is downward in other longitude regions. Typically, the equatorial ionosphere moves downward at premidnight longitudes during magnetically quiet periods [e.g., *Fejer et al.*, 1991]. Thus the vertical ion drift between the longitudes of 300° and 340°E is unusual. The enhancement of the upward drift that started before 0000 UT on the 30th is seen to be responsible for the intensification of the EIA in that longitude region. The spike-like increases in the upward velocity on orbit 2 indicate the occurrence of bubble activity in the longitude region where BPDs are detected. In the longitudinal range of 340°E–0°, the upward drift occurs at a later UT than it does west of 340°E. The uplift of the ionosphere at a later time is considered to be responsible for the bubble features detected after midnight on orbits 3 and 4. Combining the CHAMP and ROCSAT-1 observations, the *F* peak height is seen to be lifted between the CHAMP and ROCSAT-1 altitudes in the African-Atlantic sectors and above the ROCSAT-1 altitude in the American sector. The longitudinal difference of the vertical drift during storm-time is supported by the longitudinal difference in the EIA morphology observed by GUVI. The occurrence of bubbles near BPDs is explained by the enhancement of bubble activity caused by the uplift of the ionosphere. This interpretation implies that the mechanism responsible for BPDs is the cause and the nearby bubbles are the effect. *Kil and Paxton* [2006] hold the opposite view and interpret bubbles as the cause of BPDs.

Direct evidence for the uplift of the *F* peak height above the ROCSAT-1 altitude over South America is provided by the ionosonde observations at São Luis (2.5°S, 44.3°W) in Brazil. The location of São Luis is indicated with a diamond symbol in Figure 3a. The *F* peak height (hmF_2) and *F* peak electron density (NmF_2) are shown with red and blue dots, respectively. hmF_2 begins to increase at 2100 UT and reaches above 700 km at around 2300 UT. The rapid hmF_2 increase accompanies the rapid NmF_2 decrease. These observations indicate the occurrence of severe fountain process between 2100 and 2300 UT and are consistent with the GUVI observation of a wide EIA separation over South America. The data gap between 0000 and 0800 UT is attributed to the plasma density drop below the ionosonde detection limit (~2×10^4 cm^{-3}).

The observations of severe fountain process and ionospheric uplift in the region where BPDs were detected lead us to interpret the BPD phenomenon in association with the ionospheric uplift.

Penetration or disturbance dynamo electric field may be responsible for the uplift during the storm period. If storm-induced electric fields were responsible for the ionospheric uplift (or creation of BPDs), one may question how storm-induced electric fields act at a narrow longitude range confined within the BPD location. The ROCSAT-1 observation along orbit 1 in Figure 3c shows a gradual longitudinal variation of the upward plasma velocity rather than a step-like longitudinal variation. The idea of the creation of BPDs by a merger of bubbles [*Kil and Paxton*, 2006; *Kil et al.*, 2006] arose from the observation of steep walls on BPDs against the observation of a gradual longitudinal variation of the upward plasma velocity. We seek an answer to this question from the coincident occurrence of BPDs and bubbles.

The schematic diagram in Figure 5 illustrates our interpretation of the BPD morphology observed by ROCSAT-1. The ROCSAT-1 data along orbits 3 and 4 are shown as a function of magnetic longitude. The diagram indicates the existence of wave-like small-scale modulations of the *F* region height in addition to a large-scale modulation of it. The region below the *F* peak height is shown gray. The gray dotted lines indicate the composition of large- and small-scale modulations. Storm-induced electric fields may induce the large-scale modulation and cause a gradual longitudinal variation of the *F* region height. The small-scale wave-like modulations can be produced by gravity waves. Both the uplift of the ionosphere and gravity wave seeding promote the creation of bubbles. Orbit 3 passes through the wave-like modulations and depletions broader than regular bubbles are detected. Orbit 4 is below the wave-like modulations and a single broad depletion is detected. On the single broad depletion in orbit 4, a steep density gradient is formed on the west wall and a gradual variation of the density appears on the east wall. The steep density gradient on the west wall of the depletion in orbit 4 coincides with the location of a sharp depletion

in orbit 3. This observation may explain why a steep density gradient is formed on the west wall. Ignoring the walls between the three broad depletions in orbit 3, the morphology of the depletion is similar to the morphology of a single broad depletion in orbit 4. The gradual variation of the density on the east wall may represent the trough morphology in the absence of bubbles. On the other hand, the coincidence of the uplift with bubbles creates a steep density gradient on the west wall.

3.2 Observations on 24 April 2012

In the following two sections, we provide additional support for the occurrence of BPDs under the uplifted condition of the ionosphere using the coincident observations of CINDI and SSUSI. CINDI detected BPDs around 2.4 UT between the 240° and 270°E longitudes during the storm of 24 April 2012. The Dst index started to decrease at 1900 UT on the 23$^{\text{rd}}$ and reached its minimum value (-104 nT) at 0500 UT on the 24$^{\text{th}}$. The maximum Kp index was 7^{-} at 0000–0300 UT on the 24$^{\text{th}}$. Figure 6a shows the SSUSI OI 135.6 nm intensity maps on 23–25 April. The maps are the projection onto an altitude of 350 km and the observation LT is 2000. The maps on the 23$^{\text{rd}}$ and 25$^{\text{th}}$ are presented as a reference picture of what the ionosphere looked like before and after the storm, respectively. On the map on the 24$^{\text{th}}$, the C/NOFS orbit (orbit 1 in Figure 6b) on which the BPDs are detected is shown with a white solid curve. Emission depletion bands (or bubbles) appear at the location of BPDs marked with a thick white line. One difference between 24 April and the other days is that bubbles appear on the 24$^{\text{th}}$ but not on other days. Intensification of the EIA is another difference of the ionosphere on the 24$^{\text{th}}$ from that on other days.

The measurements of plasma density and vertical velocity by CINDI on the 24th are shown in Figures 6c and 6d. The latitude, LT, and altitude of the C/NOFS orbits are shown in Figure 6b. BPDs (marked in red) are detected along orbit 1 around 2000 LT and at a 400-km altitude. The plasma depletion detected near 270°E on orbit 2 may also be categorized as a BPD, although the depletion depth is much shallower than the depletions on orbit 1. In the longitude region where BPDs are detected on orbit 1, orbit 1 is closer to the magnetic equator than orbit 2 and the altitude of orbit 1 is lower than that of orbit 2. Because of the slight differences in magnetic latitude and altitude, the morphologies of plasma depletions on the two orbits are largely different. Orbit 3 crosses the magnetic equator in the longitude region where BPDs are detected on orbit 1, but the altitude of orbit 3 is about 100 km higher than that of orbit 1. **On the 24th, the EIA has already been intensified at 2.0 UT (see the GUVI swath at 2.0 UT in Figure 6a). Although we cannot identify the vertical plasma drift prior to orbit 1 from CINDI observations (data are missing), we can infer the existence of upward drift of the ionosphere before 2.0 UT from the GUVI observation. The observation of the upward drift of the background ionosphere along CINDI orbit 1 (Figure 6d) indicates that the fountain process persisted until or after 2.6 UT in some regions. In orbit 1, the creation of deep depletions at the locations where the plasma drift is downward is not explained by the instantaneous velocity. Presumably, upward plasma motion at earlier hours is responsible for those depletions.** We do not know whether bubbles existed before the detection of BPDs on orbit 1 because observations are missing. Even if observations were available for an earlier orbit, bubbles may not be detected because the sampling time is earlier than the development time of bubbles. **What we can identify from Figure 6 is the fact that the vertical background ionospheric motion was abnormal and a fountain process existed prior to the detection of BPDs.**

Figure 7 is a close-up of the observations on the 24th. The vertical white dashed lines indicate the nadir view of SSUSI. The SSUSI image marked with UT 0203 was taken about 30 min earlier than the CINDI observation on orbit 1. Three wide depletions on orbit 1 are marked with letters A, B, and C. The longitude of the dark emission depletion band (A') in the magnetic north is seen to match the longitude of depletion A. The signature of the wide density depletion B does not appear in west of the emission depletion A' on the SSUSI image, although density depletion B is detected less than 2° west from density depletion A. Many bubble signatures appear on the SSUSI image marked with UT 0334. Two emission depletion bands are clearly visible in the magnetic south on the SSUSI image. Density depletions corresponding to those emission depletion bands are not identifiable on orbits 1 and 2. At the location of density depletion C, the matching emission depletion is not visible on the SSUSI image. The absence of the signatures of wide and deep plasma depletions on the SSUSI image is difficult to explain if the formation of those depletions is associated with bubbles. One-to-one matching of the SSUSI and CINDI observations or between CINDI observations contains a certain level of uncertainty because the mapping of the SSUSI images onto an altitude of 350 km is not perfect and because the ionosphere is not stationary. **However, as the small-size density depletions between the longitudes of 290° and 295°E on two C/NOFS orbits show, bubbles are often persistent for a few hours and traceable on consecutive orbits. Although the depletions between the longitudes of 250° and 280°E are much wider and deeper compared with the depletions between the longitudes of 290° and 295°E, they are not traceable on the two consecutive orbits. We interpret that the depletions on orbit 1 were detected under the condition of orbit 3 in Figure 5. Under that condition (satellite altitude is near the bottomside), the morphology and occurrence of depletions can vary significantly for a slight difference in sampling altitude.**

3.3 Observations on 31 October 2012

The BPD event detected by CINDI on 31 October 2012 is distinguished from the BPD events reported in early sections because it is observed during a magnetically quiet time (Kp < 1^0). Figure 8 is the same format as Figure 6 for the observations on 31 October 2012. The SSUSI OI 135.6 nm maps at 2000 LT on 30 October, 31 October, and 1 November are shown in Figure 8a. The images on 30 October and 1 November are presented as a reference for the ionospheric morphology on days with no BPDs. A BPD is detected near the magnetic equator, at 2000 LT, and at a 420-km altitude on orbit 2 (Figure 8b). On orbit 1 in Figure 8c, no irregularity appears in the longitudes where the BPD is detected. The LT of orbit 1 is too early to detect irregularities. The single large BPD is detected on orbit 2, and only small magnitude density fluctuations are detected on orbit 3. Bubble features that can account for the BPD do not appear in the CINDI observations. Grown bubbles are absent in the SSUSI images. The SSUSI image at 7.4 UT was taken about an hour after orbit 2. If the BPD were associated with bubbles, bubble signatures would remain in the SSUSI image. The measurements of the vertical velocity in Figure 8d show the existence of an upward movement of the ionosphere prior to the detection of the BPD. Comparison of the SSUSI images on the three days in Figure 8a, the OI 135.6 nm intensity at the EIA location is strongest on the 31st, but the intensity at the magnetic equator is weakest on the 31st. This observation indicates that the fountain process or uplift of the ionosphere was most significant on the 31st, which is consistent with the observation of large upward velocity prior to the detection of the BPD. **The observations on the 31st again show the occurrence of a BPD when the equatorial ionosphere is uplifted.**

4. Conclusions

We have investigated the origin of abnormally broad plasma depletions (named BPDs) in the equatorial region by using the coincident optical (TIMED/GUVI and DMSP F18/SSUSI) and in situ satellite (ROCSAT-1/IPEI, C/NOFS/CINDI, and CHAMP/PLP) observations of the ionosphere on 30 May 2003, 24 April 2012, and 31 October 2012. BPDs on 30 May 2003 and 24 April 2012 are detected during geomagnetic storm periods, and a BPD on 31 October 2012 is not related to a geomagnetic storm. All the observations indicate that BPDs are a phenomenon near the magnetic equator. C/NOFS detected BPDs when its orbit is below an altitude of 450 km. The ionospheric morphology seen from the OI 135.6 nm intensity maps indicates that BPDs occur on days when strong EIAs develop. In addition to the morphology of the EIA, the observations of the upward plasma drift support the occurrence of an enhanced fountain process or uplift of the ionosphere on the days when BPD are detected. **The ionosonde observations on 29–30 May 2003 at São Luis in Brazil provide direct evidence for the uplift of the *F* peak height above an altitude of 700 km.** On the basis of these observations, we suggest that the BPD phenomena on those three days are likely caused by the uplift of the bottomside *F* region up to or above the satellite altitudes. The occurrence of bubbles by BPDs is explained by the enhancement of plasma instabilities by the uplift of the ionosphere.

Acknowledgements

W. K. Lee acknowledges support from National Radio Research Agency (2013-3-800-02). H. Kil acknowledges support from National Science Foundation Aeronomy program (AGS-1237276). CINDI data are provided through the auspices of the CINDI team at the University of Texas at Dallas supported by NASA grant NAS5-01068. Sao Luis digisonde data are courtesy of Inez S. Batista of INPE, Brazil, retrieved from the GIRO online repository at the University of Massachusetts Lowell.

References

Basu, S., et al. (2001), Ionospheric effects of major magnetic storms during the International Space Weather Period of September and October 1999: GPS observations, VHF/UHF scintillations, and in situ density structures at middle and equatorial latitudes, *J. Geophys. Res.*, *106*(A12), 30389–30413, doi:10.1029/2001JA001116.

Burke, W. J., A. G. Rubin, N. C. Maynard, L. C. Gentile, P. J. Sultan, F. J. Rich, O. de La Beaujardière, C. Y. Huang, and G. R. Wilson (2000), Ionospheric disturbances observed by DMSP at middle to low latitudes during the magnetic storm of June 4–6, 1991, *J. Geophys. Res.*, *105*(A8), 18391–18405, doi:10.1029/1999JA000188.

Burke, W. J., O. de La Beaujardière, L. C. Gentile, D. E. Hunton, R. F. Pfaff, P. A. Roddy, Y.-J. Su, and G. R. Wilson (2009), C/NOFS observations of plasma density and electric field irregularities at post-midnight local times, *Geophys. Res. Lett.*, *36*, L00C09, doi:10.1029/2009GL038879.

Christensen, A. B., et al. (2003), Initial observations with the Global Ultraviolet Imager (GUVI) in the NASA TIMED satellite mission, *J. Geophys. Res.*, *108*, 1451, doi:10.1029/2003JA009918, A12.

Fejer, B. G., E. R. de Paula, S. A. González, and R. F. Woodman (1991), Average vertical and zonal *F* region plasma drifts over Jicamarca, *J. Geophys. Res.*, *96*(A8), 13,901–13,906.

Greenspan, M. E., C. E. Rasmussen, W. J. Burke, and M. A. Abdu (1991), Equatorial density depletions observed at 840 km during the great magnetic storm of March 1989, *J. Geophys. Res.*, *96*(A8), 13931–13942, doi:10.1029/91JA01264.

Hei, M. A., R. A. Heelis, and J. P. McClure (2005), Seasonal and longitudinal variation of large-scale topside equatorial plasma depletions, *J. Geophys. Res.*, *110*, A12315, doi:10.1029/2005JA011153.

Huang, C.-S., O. de La Beaujardiere, P. A. Roddy, D. E. Hunton, R. F. Pfaff, C. E. Valladares, and J. O. Ballenthin (2011), Evolution of equatorial ionospheric plasma bubbles and formation of broad plasma depletions measured by the C/NOFS satellite during deep solar minimum, *J. Geophys. Res.*, *116*, A03309, doi:10.1029/2010JA015982.

Kelley, M. C. (2009), *The Earth's Ionosphere: Plasma Physics and Electrodynamics*, vol. 96, 2nd ed., Academic Press, Burlington, Mass.

Kil, H., and L. J. Paxton (2006), Ionospheric disturbances during the magnetic storm of 15 July 2000: Role of the fountain effect and plasma bubbles for the formation of large equatorial plasma density depletions, *J. Geophys. Res.*, *111*, A12311, doi:10.1029/2006JA011742.

Kil, H., and W. K. Lee (2013), Are plasma bubbles a prerequisite for the formation of broad plasma depletions in the equatorial F region?, *Geophys. Res. Lett.*, *40*, 3491–3495, doi:10.1002/grl.50693.

Kil, H., L. J. Paxton, S.-Y. Su, Y. Zhang, and H. Yeh (2006), Characteristics of the storm-induced big bubbles (SIBBs), *J. Geophys. Res.*, *111*, A10308, doi:10.1029/2006JA011743.

Lee, J. J., K. W. Min, V. P. Kim, V. V. Hegai, K.-I. Oyama, F. J. Rich, and J. Kim (2002), Large density depletions in the nighttime upper ionosphere during the magnetic storm of July 15, 2000, *Geophys. Res. Lett.*, *29*(3), doi:10.1029/2001GL013991.

Paxton, L. J., C. I. Meng, G. H. Fountain, B. S. Ogorzalek, E. H. Darlington, J. Goldsten, S. Geary, D. Kusnierkiewicz, S. C. Lee, K. Peacock (1992a), Special Sensor UV Spectrographic Imager (SSUSI): An instrument description, *Proc. SPIE*, 1745, pp. 2-16

Paxton, L. J., et al. (1992b), SSUSI: Horizon-to-horizon and limb-viewing spectrographic imager for remote sensing of environmental parameters, *Proc. SPIE*, *1764*, pp. 161–176.

Paxton, L. J., et al. (1999), Global Ultraviolet Imager (GUVI): Measuring composition and energy inputs for the NASA Thermosphere Ionosphere Mesophere Energitics and Dynamics (TIMED) mission, *Proc. SPIE*, *3756*, pp. 265–276.

Paxton, L. J., et al. (2002), Validation of remote sensing products produced by the Special Sensor Ultraviolet Scanning Imager (SSUSI): A far UV imaging spectrograph on DMSP F-16, *Proc. SPIE*, *4485*, pp. 338–348.

Paxton, L. J. et al. (2004), GUVI: A Hyperspectral Imager for Geospace, *Proc. SPIE*, *5660*, pp. 228–240.

Su, S.-Y., H. C. Yeh, C. K. Chao, and R. A. Heelis (2002), Observation of a large density dropout across the magnetic field at 600 km altitude during the 6–7 April 2000 magnetic storm, *J. Geophys. Res.*, *107*(A11), 1404, doi:10.1029/2001JA007552.

Sultan, P. J. (1996), Linear theory and modeling of the Rayleigh-Taylor instability leading to the occurrence of equatorial spread F, *J. Geophys. Res.*, *101*(A12), 26875–26891, doi:10.1029/96JA00682.

Zhang, Y., L. J. Paxton, J. U. Kozyra, H. Kil, and P. C. Brandt (2006), Nightside thermospheric FUV emissions due to energetic neutral atom precipitation during magnetic superstorms, *J. Geophys. Res.*, *111*, A09307, doi:10.1029/2005JA011152.

Figure Captions

Figure 1. BPDs detected by the CHAMP satellite on 30 May 2003. (a) Ground tracks of CHAMP satellite from 0.3 UT to 6.4 UT on nightside observation. The magnetic equator is indicated by the black dotted line. (b) Latitudinal profiles of the plasma density along the orbits shown in Figure 1a. LT of the CHAMP observation is around 0200. The BPD locations are indicated with thick lines.

Figure 2. Global maps of OI 135.6 nm emission observed from TIMED/GUVI during (a) quiet time (28–29 May 2003) and (b) storm time (29–30 May 2003). The maps are the projection onto an altitude of 150 km. The white dashed line represents magnetic equator. UTs given on the top of each figure are the times when the satellite passes over the geogrphaic equator. LT of the GUVI observation is around 2200. The thick white lines are the BPD locations shown in Figure 1.

Figure 3. (a) TIMED/GUVI OI 135.6 nm intensity map between 270° and 360°E longitudes on 30 May 2003. The intensity map is projected onto an altitude of 350 km. The white dotted line indicates the magnetic equator. The white solid lines indicate ground tracks of ROCSAT-1 satellite. The locations of BPDs are marked with thick white lines. (b) Ion density measurements by ROCSAT-1 along the orbits shown in Figure 3a. (c) Vertical ion velocity measurements by ROCSAT-1. The locations of BPDs are indicated with red dots in the density and velocity plots.

Figure 4. The ionosonde observations of the *F* peak height (hmF_2) and *F* peak electron density (NmF_2) on 29–30 May 2003 at São Luis (2.5°S, 44.3°W) in Brazil.

Figure 5. Schematic illustration of the BPD morphology. The gray dashed line indicates the composition of large- and small-scale modulations.

Figure 6. (a) DMSP/SSUSI OI 135.6 nm intensity maps on 23 April 2012 (left), 24 April 2012 (center), and 25 April 2012 (right). The white dotted lines indicate the magnetic equator. (b) Latitude, LT, and altitude of C/NOFS on April 24. (c and d) Measurements of the ion denisty and vertical ion velocity by CNOFS/CINDI along the orbits shown in Figure 4b. The locations of BPDs are identified with red dots.

Figure 7. (top) Close-up of DMSP/SSUSI OI 135.6 nm map on 24 April 2012. The white dashed lines indicate DMSP orbits. The white solid lines indicate ground tracks of C/NOFS. (bottom) CNOFS/CINDI ion density measurements along the orbits indicated on the top image.

Figure 8. (a) DMSP/SSUSI OI 135.6 nm intensity maps on 30 October 2012 (left), 31 October 2012 (center), and 1 November 2012 (right). (b) Latitude, LT, and altitude of C/NOFS on 31 October. (c and d) Measurements of the ion denisty and vertical ion velocity by CNOFS/CINDI along the orbits shown in Figure 6b. The locations of BPDs are identified with red dots.

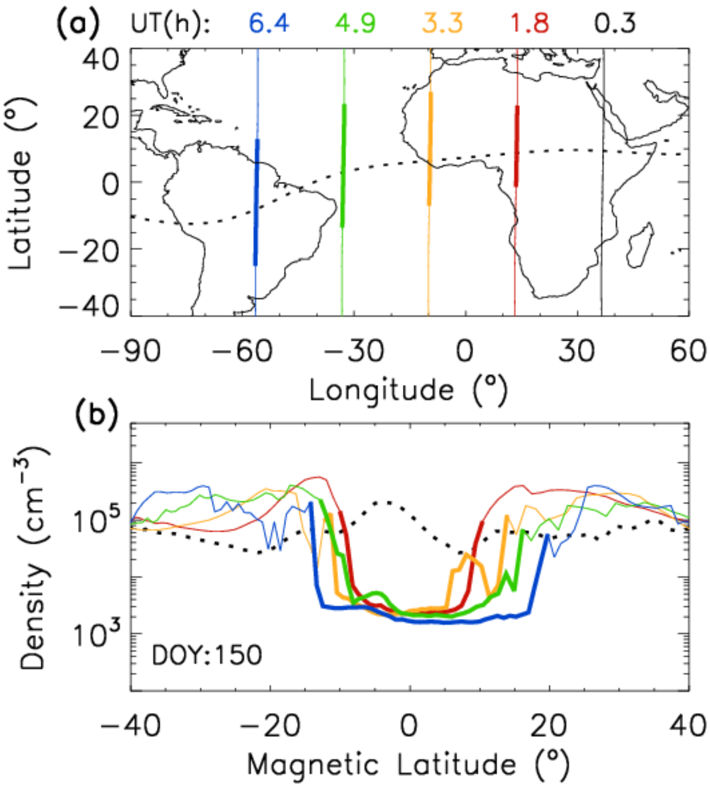

Figure 1. BPDs detected by the CHAMP satellite on 30 May 2003. (a) Ground tracks of CHAMP satellite from 0.3 UT to 6.4 UT on nightside observation. The magnetic equator is indicated by the black dotted line. (b) Latitudinal profiles of the plasma density along the orbits shown in Figure 1a. LT of the CHAMP observation is around 0200. The BPD locations are indicated with thick lines.

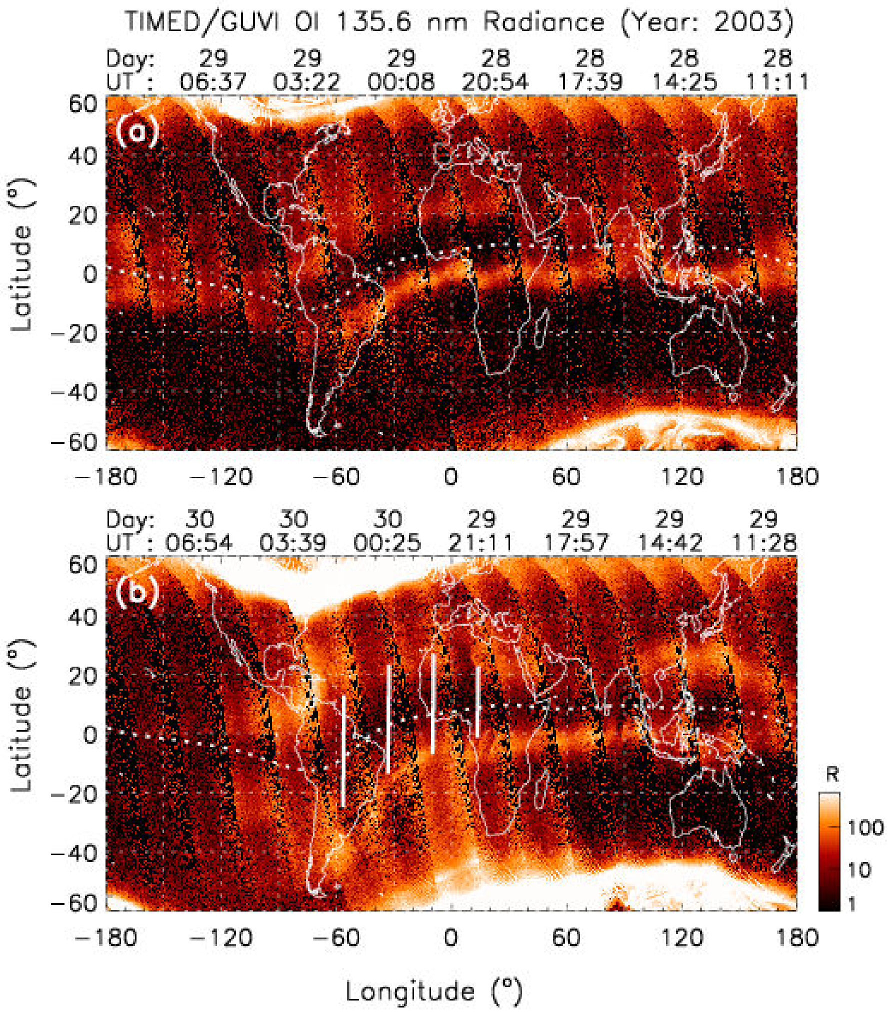

Figure 2. Global maps of OI 135.6 nm emission observed from TIMED/GUVI during (a) quiet time (28–29 May 2003) and (b) storm time (29–30 May 2003). The maps are the projection onto an altitude of 150 km. The white dashed line represents magnetic equator. UTs given on the top of each figure are the times when the satellite passes over the geogrphaic equator. LT of the GUVI observation is around 2200. The thick white lines are the BPD locations shown in Figure 1.

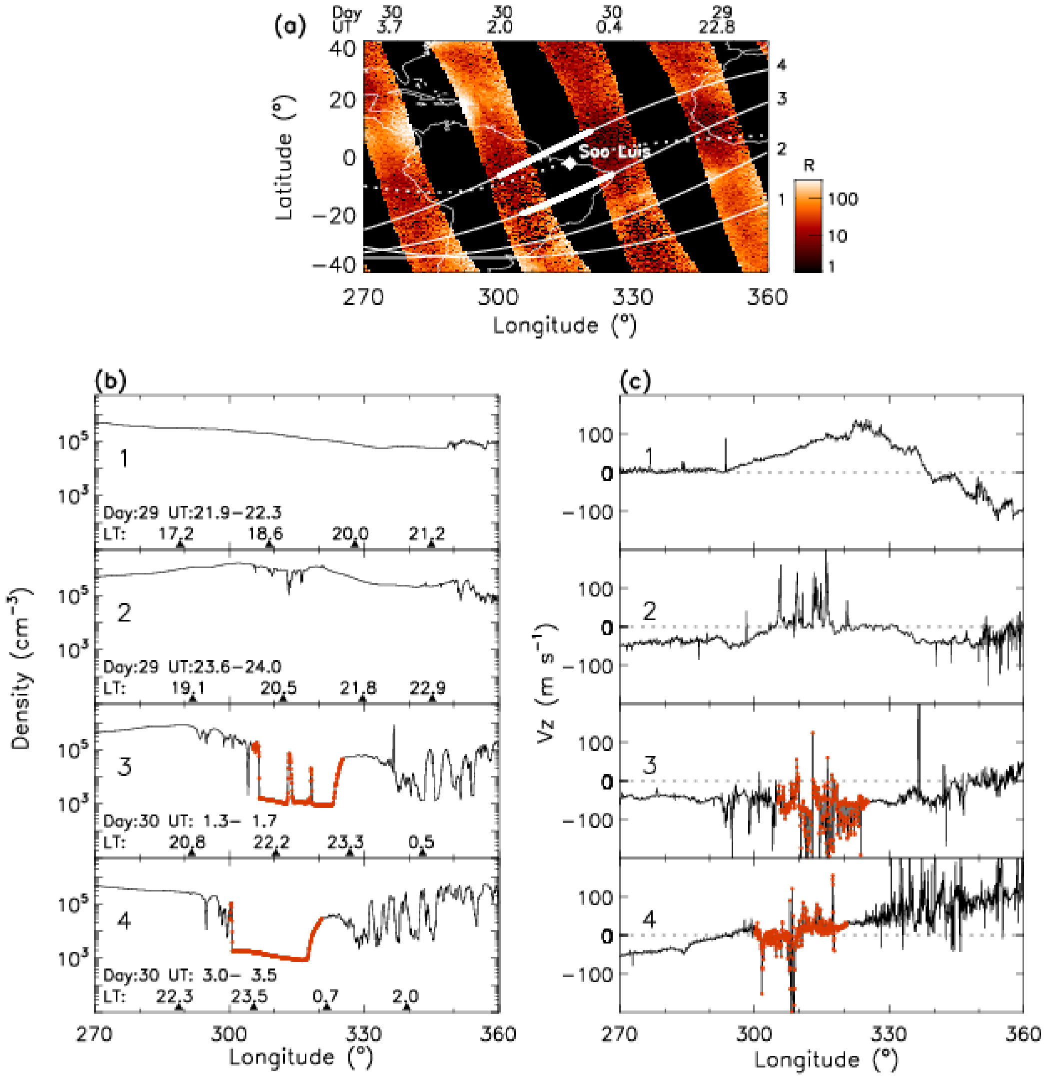

Figure 3. (a) TIMED/GUVI OI 135.6 nm intensity map between 270° and 360°E longitudes on 30 May 2003. The intensity map is projected onto an altitude of 350 km. The white dotted line indicates the magnetic equator. The white solid lines indicate ground tracks of ROCSAT-1 satellite. The locations of BPDs are marked with thick white lines. (b) Ion density measurements by ROCSAT-1 along the orbits

shown in Figure 3a. (c) Vertical ion velocity measurements by ROCSAT-1. The locations of BPDs are indicated with red dots in the density and velocity plots.

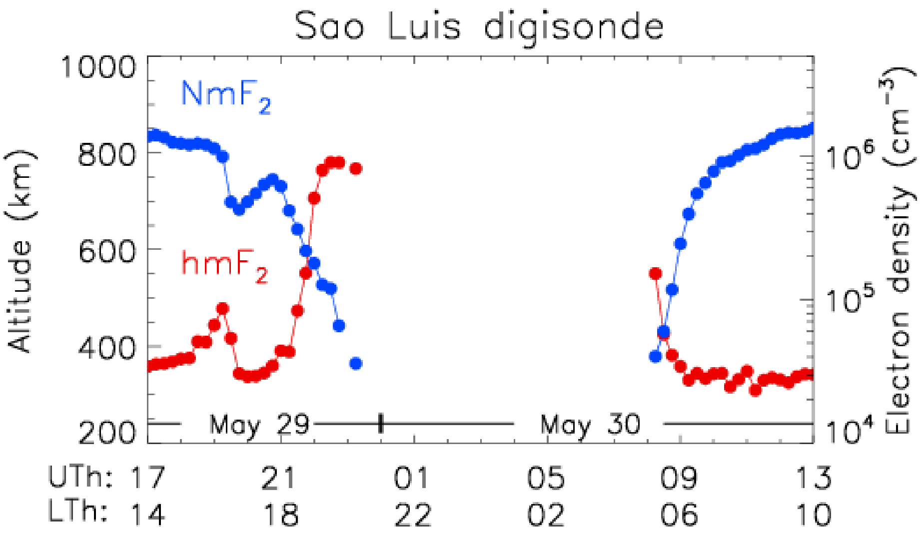

Figure 4. The ionosonde observations of the *F* peak height (hmF_2) and *F* peak electron density (NmF_2) on 29–30 May 2003 at São Luis (2.5°S, 44.3°W) in Brazil.

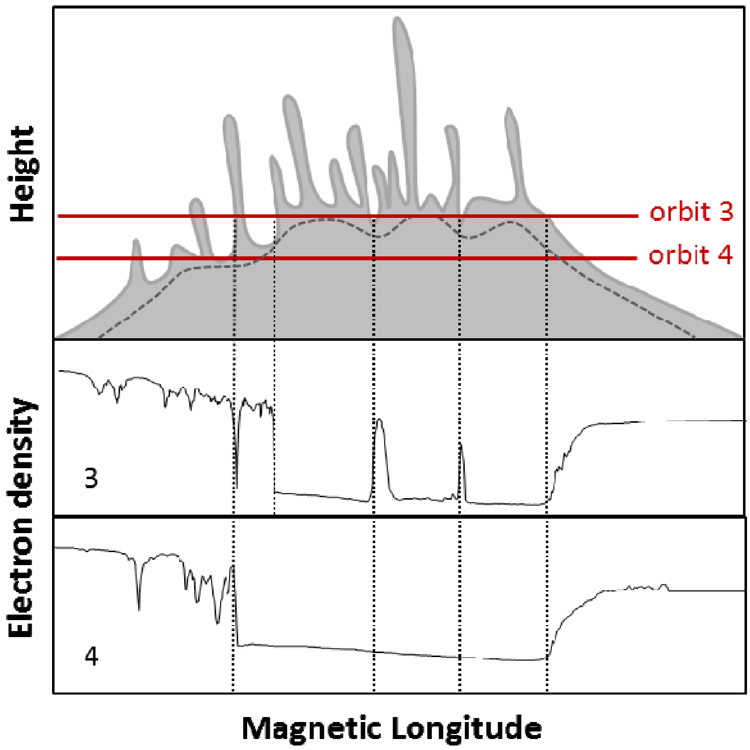

485 **Figure 5.** Schematic illustration of the BPD morphology. The gray dashed line indicates the
486 composition of large- and small-scale modulations.

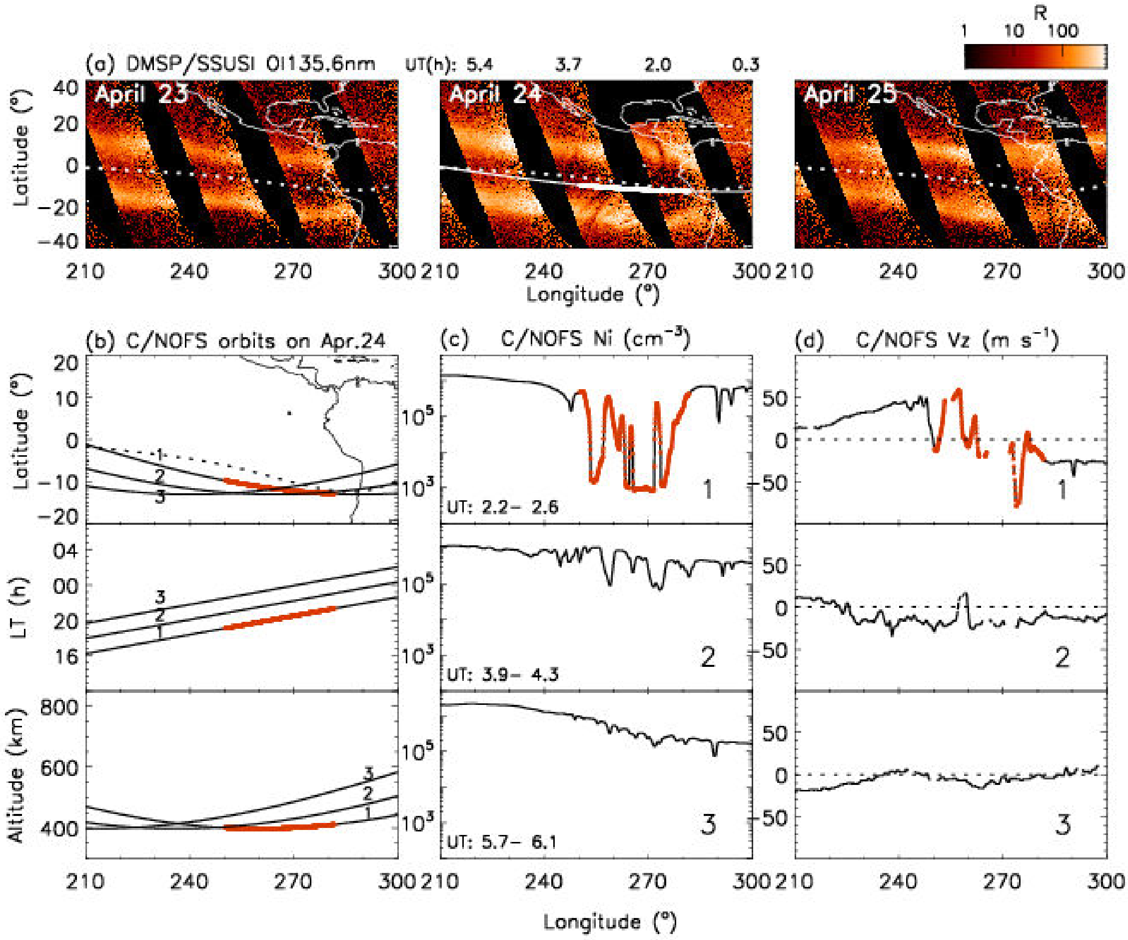

Figure 6. (a) DMSP/SSUSI OI 135.6 nm intensity maps on 23 April 2012 (left), 24 April 2012 (center), and 25 April 2012 (right). The white dotted lines indicate the magnetic equator. (b) Latitude, LT, and altitude of C/NOFS on April 24. (c and d) Measurements of the ion denisty and vertical ion velocity by CNOFS/CINDI along the orbits shown in Figure 4b. The locations of BPDs are identified with red dots.

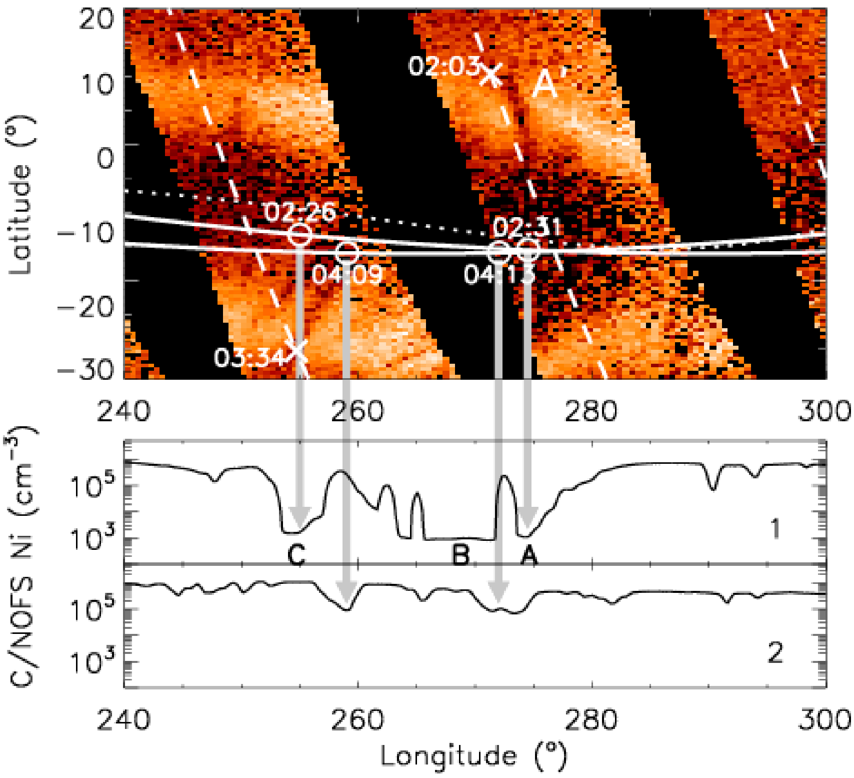

Figure 7. (top) Close-up of DMSP/SSUSI OI 135.6 nm map on 24 April 2012. The white dashed lines indicate DMSP orbits. The white solid lines indicate ground tracks of C/NOFS. (bottom) CNOFS/CINDI ion density measurements along the orbits indicated on the top image.

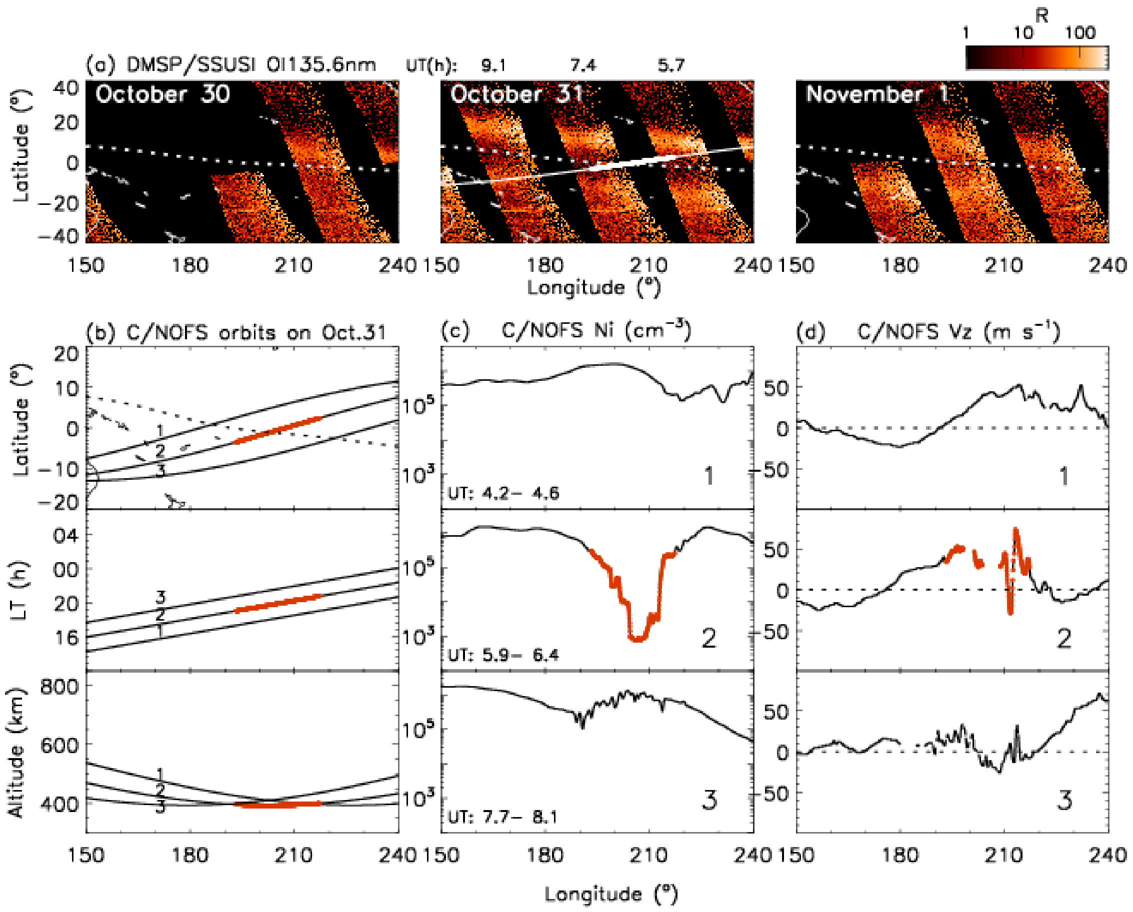

Figure 8. (a) DMSP/SSUSI OI 135.6 nm intensity maps on 30 October 2012 (left), 31 October 2012 (center), and 1 November 2012 (right). (b) Latitude, LT, and altitude of C/NOFS on 31 October. (c and d) Measurements of the ion denisty and vertical ion velocity by CNOFS/CINDI along the orbits shown in Figure 6b. The locations of BPDs are identified with red dots.